Proceedings of The Magnetized Plasma in Galaxy Evolution
Sep. 27th – Oct. 1st 2004, Jagiellonian University, Kraków, Poland
Eds. K.T. Chyży, K. Otmianowska-Mazur, M. Soida and R.-J. Dettmar

The dispersion and symmetry characteristic of MRI-driven turbulence in ISM

Natalia Dziourkevitch

Max-Plank Institute for Astronomy, Königstuhl 17, D-69117 Heidelberg

Abstract

The nonlinear evolution of magneto-rotational instability (MRI) is investigated in the galactic disks. The model includes differential rotation, vertical density stratification, no self-gravitation. The full set of MHD equations is solved, using 3D ZeusMP code. The global simulations are presented for the cylindrical computational box where both rigid and flat parts of rotation curve are included. Calculations show that the MRI-driven turbulence first appear in the inner part of a sheared disk and slowly propagates outwards. The growth rate is shown to depend on the shear rate. We justify the idea of explaining the observed dispersion velocity value (common for many galaxies) with the MRI action in sheared outer disk (Sellwood & Balbus 1999), obtaining the velocity dispersion ~ 5 km/s. The radial dependence of growth rates, velocity dispersion and magnetic pitch angles in the galaxy are demonstrated.

1 Introduction

In the Milky Way the line widths of individual molecular and HI clouds and cloud complexes exceed the expected thermal width according to estimated kinematic temperatures. The 21 cm dispersion does not drop below 5–7 km/s, regardless of how low the optical surface brightness becomes. Obviously, interstellar turbulence does not decay in regions without star formation activity. A local analytical study of magneto-rotational instability (MRI) and MRI-driven turbulence acting in a disk were applied to the particular case of NGC 1058, a face-on disk galaxy with a well-studied extended HI disk (Sellwood & Balbus 1999). This implied a magnetic field of about 3 μG which well agrees with observed field strength of many galaxies. The feedback of the MRI-driven magnetic fields onto the density field and velocity flows should be studied numerically and in the global models.

Magneto-rotational instability (MRI) is a flexible and fast mechanism to generate the strong (few μG) magnetic fields. MRI is free to appear under most galactic physical conditions with the only requirement: the angular frequency of galactic rotation decreasing outwards. The condition is fulfilled for *any* spiral galaxy. The energy source for MRI is the differential rotation. A very weak (external) vertical magnetic field $\sim 10^{-25}$G is enough for the instability to operate (Kitchatinov et al. 2004).

A seed field in the early universe is given as 10^{-18}G (Hanasz & Lesch 1997). The typical growth rate of a dynamo is ≤ 1 Gyr^{-1}. As an example, after 2.5 Gyr the field will be amplified from 10^{-8}G to 10^{-6}G only. Therefore, the initial fields for a dynamo should be larger than 10^{-8}G. It is in no contradiction with observations, thought one must explain which fast mechanism has amplified the the magnetic fields to 10^{-8}G.

The *quadrupolar* magnetic field geometry is developed by MRI from the vertical initial or external field due to the differential rotation (Dziourkevitch et al, 2004). Even when MRI action is disturbed by the SN, the magnetic seed field driven by MRI has the ideal properties for further dynamo operation.

The nonlinear winding up of the seed field can give the observable magnetic fields and correct pitch angles only for times much shorter than 1 Gyr. The seed field would decay quickly. The life-time is 210 Myr according to Rohde et al. (1998), 200 Myr is the result of Otmianowska-Mazur & Chiba (1995) which is similar to Parker's estimate (1979). In early epoch the magnetic fields are placed between the optical arms, what fits to observations. Rather quickly, however, the magnetic arms are winded up till pitch angle is zero. The pitch angles reach zero faster than the magnetic fields decay.

The questions for MRI to be applied are the following. The high velocity dispersion in the outer part of the NGC 1058 disk (~ 10 kpc) shall be explained. The question of fast (1–2 Gyr) magnetic field amplification with obtaining the large pitch angles is still actual.

2 Problem description

The system of magneto-hydrodynamical equations

$$\frac{D\rho}{Dt} + \rho\nabla \cdot \mathbf{u} = 0, \tag{1}$$

$$\rho\frac{D\mathbf{u}}{Dt} = -\nabla P - \rho\nabla\Psi + \frac{1}{4\pi}(\nabla \times \mathbf{B}) \times \mathbf{B}, \tag{2}$$

$$\frac{\partial \mathbf{B}}{\partial t} = \mathrm{curl}\,(\mathbf{u} \times \mathbf{B} - \eta \mathrm{curl}\mathbf{B}) \tag{3}$$

are solved with help of 3D ZeusMP using the uniform grids. The feedback of magnetic fields $\mathbf{B}$ onto velocity fields $\mathbf{u}$ is included as a Lorentz force in Navier-Stokes equation. The isothermal relation $P = c_\mathrm{s}^2\rho$ with the sound speed $c_\mathrm{s} = 10$ km/s is used for the interstellar medium. Magnetic diffusivity η is a rather small value for a warm gas component of the ISM (Kitchatinov et al. 2004).

The resolution is chosen to keep from 8 to 11 grid points for resolving the most unstable wavelength, which value was calculated according to Balbus & Hawley (1991a, 1991b). Artificial viscosity is introduced in every model. It dissipates high-frequency numerical noise and smears out shock fronts if the flow becomes supersonic.

3D global simulations in the cylindrical coordinates have been done for a disk of thickness $Z = [-1, 1]$ kpc and $R = [1, 5]$ kpc. The gravitation potential Ψ is assumed to be generated by the stellar population, self-gravity of the gas is not included. We have prescribed the potential Ψ for radial and vertical directions separately so that similar shape in stratification and rotation curve profile result following Fröhlich & Schultz (1996). No azimuthal variations like density waves and spirals are introduced. All non-axisymmetric structures in density or flow and fields in the simulations are thus due to MRI. The rotation curves are described via Brandt-type rotation law

$$u_\phi = \frac{R\;\Omega_0}{(1 + (R/R_0)^n)^{1/n}}, \tag{4}$$

where R_0 is the radius of transition from rigid to differential rotation, Ω_0 is the angular frequency of rigid galactic "core" rotation, factor $n = 2$ or $n = 4$. Lacking knowledge about the vertical stratification of the gas density in considered galaxies we adopt the empirical HI distribution of Dickey & Lockmann (1990) for our Galaxy: a combination of two Gaussian

Table 1: Density-stratified models with different rotation laws

model	R_0 [kpc]	Ω_0 [Gyr^{-1}]	n	B_z [μG]	$u_{\rm T}$ [km/s]	$B_{\rm T}$ [μG]	$V_{\rm A,T}$ [km/s]
U1	2.00	76	2	0.32	5.8	1.4	24
U2	1.00	152	2	0.32	4.2	0.9	19
U3	1.52	100	4	0.32	6.7	1.2	34
U4	2.80	53	4	0.32	4.3	1.5	15

Table 2: Simulation results e-folding time of magnetic field T and the ratio of magnetic to kinetic energy. Parameter $2\pi/\Omega_0$ is a e-folding time estimation following the idea of Kitchatinov et al. (2004)

model	$2\pi/\Omega_0$ [Myr]	T [Myr]	$E_{\rm mag}/E_{\rm kin}$
U1	82	81	3.6
U2	41	44	4.6
U3	63	46	3.0
U4	119	96	2.9

functions $\exp(-z^2/H^2)$ with central densities 0.395 and 0.107 cm^{-3} and scale heights of 212 and 530 pc, respectively, and an exponential function $\exp(-|z|/H)$ with central density 0.064 cm^{-3} and a scale height of 403 pc.

3 Results

The models with different rotation curves are presented in Table 1. The variations of the Brandt-type rotation curve parameters R_0, Ω_0 and n (Eq.(4)) are given in the first three columns. Initial magnetic field is purely vertical and homogeneous everywhere in the disk with the corresponding Alfvén velocity $V_{\rm A,0} = B_z/\sqrt{4\pi\rho(z)}$ ($\rho = 10^{-24}$gcm^{-3} at the galactic midplane). The following columns in the Table 1 are, consequently, the velocity dispersion $u_{\rm T} = \sqrt{\langle \boldsymbol{u}'^2\rangle}$, the amplitude of the turbulent magnetic fields $B_{\rm T} = \sqrt{\langle \boldsymbol{B}'^2\rangle}$ and the Alfvén velocity dispersion $V_{\rm A,T} = \sqrt{\langle \boldsymbol{V}'^2_{\rm A}\rangle}$. $\boldsymbol{u}'$, $\boldsymbol{B}'$ and $\boldsymbol{V}'_{\rm A}$ are the turbulent fluctuations of the fields. The resolution is [256 : 512 : 256] for the disk with half-thickness H = 1kpc and the radius from 1kpc to 5kpc. Exception is the model U4 for it has extended radius from 1kpc till 11kpc with resolution of [256 : 1024 : 256] mesh points. The perfect conductor boundary condition in the radial direction was used for all models, with reflective (pseudo-vacuum) vertical boundaries.

Models U[1-4] are made to fit the rotation curve of NGC 1058, the galaxy with extended HII disk and unclear rotation law. Models U4 and U1 are the best fits for the observed rotation curve by Dickey et al. (1990) assuming the inclination $\sin i = 0.1$. Still, keeping in mind the possible warping of the disk we calculated the curves with very different behavior inside the radius $R \leq 7$ kpc. Parameters R_0, Ω_0 and n are varied, what directly affects the radial dependence of the shear.

Topology and global symmetries. The MRI-driven turbulence appears to have a sheets-like structure in edge-on disks (Fig. 1). The vertical length of the turbulent cells is smaller by order of magnitude compared to the radial one. Both length-scales vary during the simulations. The cells evolve from small to large structures. The influence of the density stratification is visible both in the initial and the final stages. The smallest scales belong to the region of the maximal density at the equatorial plane ($z = 0$ kpc) and they are most visible at earlier times, whereas at the last stage of MRI development the turbulence is present at all heights with slight differences in cell thickness. The sheets are lying parallel to the disk plane almost without mixing vertically.

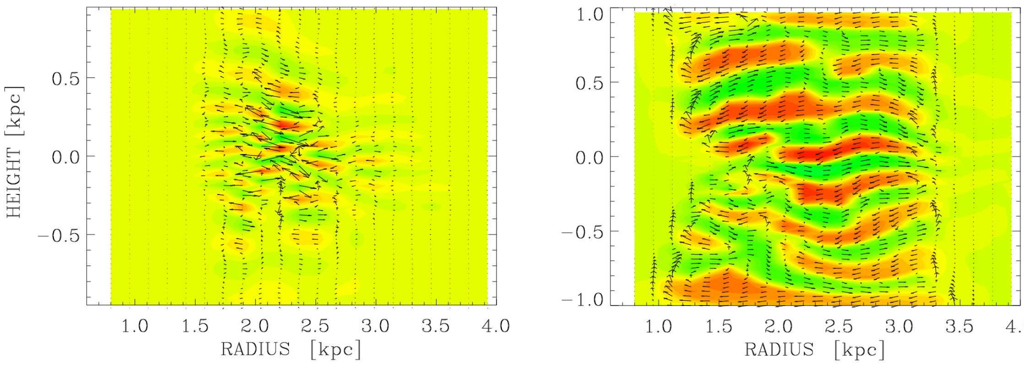

Figure 1: Plots 2a) and 2b) represent the model U3 for time slices $t = 0.6$Gyr and $t = 0.9$Gyr. The minima and maxima of the B_ϕ components are shown in green and red colors (dark shadows at the no-color print). Gray (yellow) is a mark of vanishing B_ϕ component. Overplotted arrows show radial and vertical components of the magnetic field for same time slices.

Comparison of stability diagrams for the dipolar and quadrupole magnetic patterns from the linear global model of Kitchatinov & Rüdiger (2004) shows that one could not exclude the mixed parity to appear in the nonlinear regime. The final configuration due to MRI is a mixed mode, as it was shown in Dziourkevitch et al. (2004). The same remains true for presented models.

Growth rates. The fastest growing instability we get for model U2, which has the highest $q\Omega_0$. Global e-folding time is about 44 Myr (Table 2). As we can see from Table 1 and Table 2, the prediction of $\gamma_{\rm global} = 1/\tau_{\rm rot} = \Omega_0/2\pi$ (Kitchatinov et al. 2004) is valid only for the model which has the $n = 2$ for rotation law (models U1 and U2). Models U3 and U4 show other rule for growth rates.

The disk can be represented as a superposition of rings with thickness $\Delta R = 0.3$kpc. The growth rates for every ring are calculated (Fig. 2). The maximal growth rate of 25 Gyr^{-1} (model U2) appears at the radius 1.2kpc what is very close to the transition radius $R_0 = 1$ kpc (Fig. 2). It is obvious that the growth rate radial dependence is reflecting the radial behavior of shear. Fig. 2 shows that the magnetic field is developing a bit slower outside of the disk.

Velocity dispersion: radial and vertical behavior. It is not surprising then that the velocity dispersion appears to be strongly dependent on radius too (Fig. 3). Nevertheless, from ob-

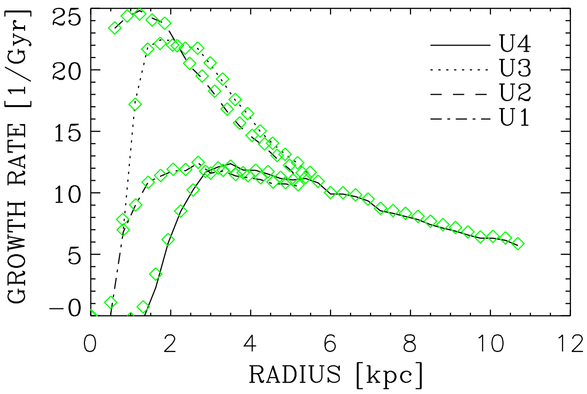

Figure 2: The growth rates for B_ϕ (different lines, see notation in the plot) and B_r (rhombs) for models in Table 2

servations of NGC 1058 we know that it drops from 12 km/s to 6 km/s at the inner part ($1 \leq R \leq 5$ kpc), then up to $R \simeq$ 11kpc u_{T} is almost fixed at about 5.7 km/s. MRI appears to be the mechanism to explain the magnitude of velocity dispersion. From the radial behavior of growth rates we are now able to estimate the times needed for the saturation of the turbulence at the different radii. For example, in our best-fit model U4 the disk part with radii between 3 and 6 kpc has a developed turbulence after 1.3 Gyr, whereas the outer part ($>$ 10 kpc) will need 2.7 Gyr to reach the same amplitudes. The shape of the turbulent velocity radial distributions (see Fig. 3) will change with time towards widening and flattening of the profile. The average turbulence intensity slightly exceeds the value of 5 km/s. The characteristic amplitude of the magnetic field fluctuations is about 1 μG.

Pitch angles: temporal and spatial behavior. The magnetic fields are showing a pitch angle of about $-30^{\rm o}$ (Fig. 3). There is no difference in pitch angle behavior above or below equator. Magnetic field strength (over-plotted with dots) has strong dependence on radius, having it's maximum near the transition radius R_0 while the pitch angles decrease in absolute value. Interesting, that the high pitch angles are existing only for not-saturated MRI. For galaxy it's a sufficiently long time (1-2 Gyr). After the saturation the pitch angle drops till values of $-1^{\rm o}$.

4 Conclusions

Our main results are following. The model reproduces the observed rms values of magnetic fields and velocity dispersion of ISM. We have confirmed the prediction of Sellwood & Balbus (1999) that the turbulent velocity dispersion is linked to the Alfvén speed. The dispersion of about 5 km/s is typical for the magnetic shear instability in galaxies. MRI has strong radial dependence of the growth rate and, consequently, of the turbulence. The constancy of velocity dispersion in the NGC 1058 outer disk can be explained if the galaxy was unperturbed over at least 3 Gyr.

MRI transports the energy from small to large scales. The final structure (if not disrupted

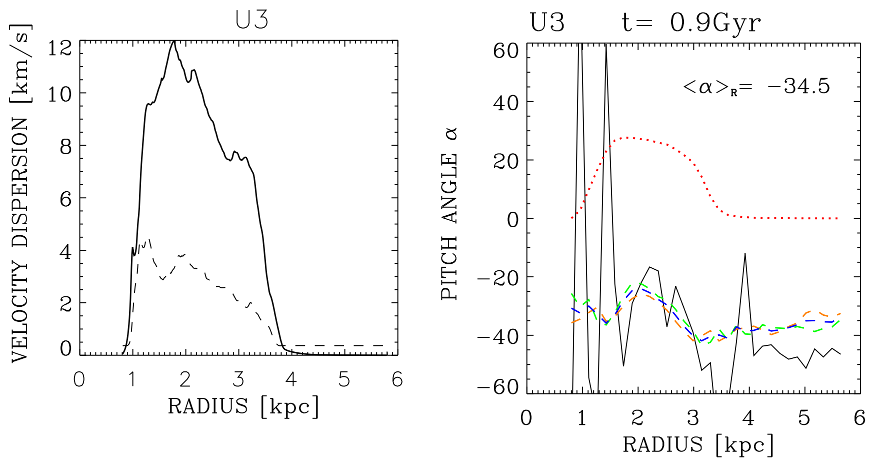

Figure 3: Left: The radial dependence of the turbulent intensity u_{T} (solid line for in-plane and dashed line for vertical dispersion). Right: The averaged pitch angle $\langle\alpha\rangle_{Z,\phi}$ is shown with grey (average over northern/southern hemidisk) and black (full average) dashed lines. Dotted line is representing the absolute value of the magnetic field $\left(10 \times \langle B_R^2 + B_\phi^2\rangle^{1/2}_{Z,\phi}\ \mu\mathrm{G}\right)$

by SN) is the pack of 'thin layers' (thin means 100 parsecs at least), what can lead to application to the proto-stellar cloud formation.

The MRI is shown to be a very fast instability with e-folding time of $\tau_{\mathrm{rot}} = 2\pi/\Omega_0$, for the Brandt type rotation law with n=2. More steep rotation curves have the faster magnetic energy growth. The growth rates can be locally estimated for any fixed radius using the local theory predictions. MRI easily could explain the existence of rather large magnetic fields in very young galaxies.

The magnetic fields have many reversals between the rings, but the averaged pitch angle is always negative with an amplitude of about $-30°$. Minimum of MRI-driven pitch angle is corresponding to the strongest B_ϕ component and placed at the transition radius R_0. Strong pitch angle is observed only for non-saturated MRI. The influence of the magnetic diffusion and SN explosions on the saturation rate shall be investigated.

References

Dickey, J.M., Hanson, M.M., Helou, G., 1990, ApJ, 352, 522

Dickey, J.M., & Lockman, F.J., 1990, ARA&A, 28, 215

Dziourkevitch, N., Elstner, D., Rüdiger, G., 2004, A& A, 423, L29

Hanasz, M., Lesch, H., 1997, A&A, 321, 1007

Kitchatinov, L., Rüdiger, G., 2004, A&A 424, 565

Otmianowska-Mazur, K., Chiba, M., 1995, A&A 301, 41

Parker, E.N., 1979, Cosmical Magnetic Fields: Their Origin and Their Activity, Oxford Univ. Press

Sellwood, J.A., Balbus, S.A., 1999, ApJ, 511, 660

Rohde, R., Elstner., D., 1998, A&A, 333, 27